Indian Journal of Chemistry
Vol. 56A, October 2017, pp. 1007-1013

Electrodeposition of platinum-iridium nanoparticles on carbon nanotubes and their electrocatalytic oxidation of glucose

Bohua Wu[a,*], Jiajin Zhu[a], Xue Li[a], Ting Zhou[b], Liqiu Mao[b] & Shanxin Xiong[a]

[a]College of Chemistry and Chemical Engineering, Xi'an University of Science & Technology, Xi'an, 710054, PR China
Email: wubohua2005@126.com

[b]National & Local Joint Engineering Lab. for New Petro-Chemical Materials and Fine Utilization of Resources, College of Chemistry and Chemical Engineering, Hunan Normal University, Changsha 410081, PR China

Received 1 May 2017; revised and accepted 22 September 2017

Platinum-iridium (PtIr) nanoparticles (NPs) have been anchored on the surface of carbon nanotubes by potentiostatic electrodeposition in 0.5 *M* H_2SO_4+0.5 *M* glycerol aqueous solution. The surface and composition of the PtIr NPs/CNTs nanohybrids have been characterized by transmission electron microscopy and energy dispersive spectroscopy, respectively. The electrocatalytic properties of the PtIr NPs/CNTs catalysts for glucose oxidation have been investigated by cyclic voltammetry and chronoamperometry. The size of the PtIr NPs can be controlled from 3.0–7.0 nm by controlling the amount of Ir. In particular, the PtIr NPs has been optimized at 1:1 Pt/Ir atomic ratio. The as-prepared PtIr (1:1) NPs/CNTs catalysts possess unique properties including small size of PtIr NPs, excellent dispersion, high electrochemical active surface area and exhibit high activity towards glucose oxidation. For comparison, Pt NPs/CNTs catalysts have also been prepared under the same controlled procedure. In the absence of Ir, Pt NPs are also uniformly dispersed on the CNTs, and their average diameter is 4.0±0.5 nm, close to that of PtIr NPs. Further, addition of Ir makes PtIr (1:1) NPs/CNTs catalysts superior to Pt NPs/CNTs catalysts in term of better long-term stability and higher catalytic efficiency of glucose oxidation. The PtIr (1:1) NPs/CNTs catalysts are proved to be promising anode catalysts for direct glucose fuel cells.

Keywords: Fuel cells, Electrocatalytic oxidation, Oxidation, Glucose oxidation, Electrodeposition, Anode catalysts, Carbon nanotubes, Platinum alloy, Iridium

Glucose is the most richly found monosaccharide in nature and its complete oxidation can produce high energy (2.87×10^3 kJ mol^{-1})[1]. To gain access this energy, use of glucose fuel cells for direct conversion of chemical energy to electric energy is a promising alternative. Therefore, electrochemical oxidation of glucose has attracted wide interest because of the high potential of direct glucose fuel cells[2, 3]. It is well-known there are two routes for fabricating the anode for efficient oxidation of glucose at low over-potentials. One is using metal or metal alloys electrocatalysts, mostly in alkaline medium with compartmentalization of the electrodes[4-7], and the other is using redox enzymes such as glucose oxidases or dehydrogenases[8-12], at natural pH without any compartmentalization. Enzymes electrodes take advantage of the high selectivity toward their substrates, but the grafting of enzymes onto electrodes is difficult, which hinders the efficient electron transfer to the enzymes redox active site. However, the application of enzymes electrodes is limited by their poor thermal and chemical stabilities as well as complex immobilization procedures that may further decrease the stability of enzyme[8, 9, 12].

On the other hand, noble metal nanocrystals, such as Au, Pd, and Pt[2, 13, 14], have been intensively studied in fuel cells because of their excellent electrocatalytic activity towards different types of fuels. Among these noble metal electrocatalysts, Pt and Pd are the initially explored materials for glucose electrooxidation[15], including Pt/C[16], Pd/C[17], Pt/MWCNTs[18], Pd/MWCNTs[19], etc. However, due to the high cost and poor activity of Pt, being easily subjected to poisoning by absorbed intermediates during the glucose oxidation process[20], it is not an ideal anode catalyst for glucose fuel cell applications. Gold-containing catalysts such as Au/C[21], Au/CNTs[22], Au-Ag[23] have also been receiving attention. To mitigate the poisoning problem and accelerate the glucose oxidation, some Pt-based bimetallic catalysts, such as Pt-Pb[24], Pt-Au[2], Pt-Ru[25, 26], Pt-Ni[27], Pt-Ir[28, 29] have been developed, which exhibited considerable advantages compared to Pt. Recently research has

shown that iridium can absorb hydroxyls on the oxophilic Ir at a low potential for removal of CO species and has a relatively high oxidation potential of 1.156 V (Ir^{3+}/Ir)[29]. Adding Ir to Pt can make it more resistant to poisoning and metal dissolution under fuel cells conditions. Therefore, Ir can effectively improve the performance of Pt catalysts in the glucose electrooxidation reaction.

It is well-known the catalytic activity of metal nanoparticles (NPs) is strongly related to their particle size, distribution, and support materials[30]. Usually, highly conductive supports with high specific areas play a critical role in the high utilization of noble metal catalysts for both low cost as well as good catalytic activity. Pt and Pt alloys are generally supported by various carbon materials including carbon black[31], grapheme[32], graphite nanofibers[33] and carbon nanotubes (CNTs)[28]. Among these carbon materials, CNTs have been proven to be good support for both enzymes and metal catalysts due to their high specific surface area, excellent electronic conductivity, and outstanding chemical and electrochemical stability[30]. Therefore, high dispersion of PtIr NPs supported on CNTs is expected to provide superior electrocatalytic activity towards the glucose oxidation. However, to the best of our knowledge, there are only a few reports on the synthesis of CNT-supported PtIr NPs[29] because of the high heat formation energy of PtIr NPs and the insert graphitic surface of CNTs.

Electrodeposition is one of the most efficient methods for formatting and synthesizing metal NPs since it is rapid and easy, and allows easy control of the nucleation and growth of metal NPs[34]. Herein, highly dispersed PtIr NPs with varied compositions on CNTs were prepared by a modified electrodeposition method. To control the particle size of PtIr NPs on CNTs, glycerol was added to the electrolyte to increase its viscosity. In addition, we also optimized the ratio of Pt and Ir in PtIr NPs by adjusting the molar ratios between the metal precursors (H_2PtCl_6 and H_2IrCl_6) in the electrolyte solutions to enhance the electrocatalytic performance on glucose oxidation. Electrochemical and physical characterizations of the prepared catalysts have been done by cyclic voltammetry (CV), chronoamperometry (CA), energy dispersive spectroscopy (EDS), inductively coupled plasma-atom emission spectroscopy (ICP-AES) and transmission electron microscopy (TEM).

Materials and Methods

Pristine multi-walled carbon nanotubes (CNTs) (length 5-15 μm, diameter 20-60 nm) was purchased from Shenzhen Nanotech Port Co. Ltd., China, chloroplatinic acid (H_2PtCl_6) and dihydrogen hexachloroiridate hydrate ($H_2IrCl_6 \cdot 6H_2O$) were purchased from Alfa Aesar, and Nafion ethanol solution (5.0 wt.%) was bought from Sigma Aldrich. Other chemicals were of analytical grade and used as received. Deionised water was used to prepare samples or solutions, while ultra-pure N_2 was used for the deaeration of the electrolytes.

Electrode preparation

A glassy carbon (GC, 5 mm diameter) electrode was polished with the slurry of 0.5 and 0.03 μm alumina successively and washed ultrasonically in deionised water prior to use. The CNTs were pretreated by refluxing in a mixed acid (H_2SO_4:HNO_3 in 1:3 *v/v* ratio) solution at 140 °C for 5 h, followed by washing and vacuum drying at 80 °C overnight.

The CNTs ink was prepared by dispersing 4 mg of the ground CNTs in 4 mL of deionised water by sonication. When a dark homogeneous dispersion was formed, 40 μL of ink was dropped onto the surface of the GC electrode using a microsyringe. After drying under an infrared lamp, the electrode was coated with 10 μL of 0.05 wt.% Nafion ethanol solution to fix the CNTs.

Deposition of PtIr NPs on CNTs

PtIr NPs were deposited on the CNTs with a CHI 660C electrochemical workstation (CH Instrument, China). A standard three-electrode cell was used with the CNTs/GC electrode as the working electrode, a platinum wire as the counter electrode, and a saturated calomel electrode (SCE) as the reference electrode.

PtIr NPs were electrodeposited on CNTs/GC electrode by potentiostatic method in 0.5 *M* H_2SO_4+0.5 *M* glycerol aqueous solution containing H_2PtCl_6 and H_2IrCl_6. The deposition potential was -0.25 V. In the electrolyte solution, the concentration of H_2PtCl_6 was kept constant (1.3 m*M*) and that of H_2IrCl_6 was varied from 0.43 m*M* to 3.9 m*M*. The atomic ratios of Pt to Ir ($R_{Pt/Ir}$) were kept at 3:1, 1:1, 1:3. Before PtIr NPs deposition, the electrolyte was bubbled with ultra-pure nitrogen gas for 15 min for deaeration. After deposition for 30 min, the obtained electrode was immersed in hot water for at least 2 h to completely remove any potentially adhering glycerol or metal precursors from the CNTs network. The prepared catalysts on electrodes were labeled as PtIr (3:1) NPs/CNTs, PtIr

(1:1) NPs/CNTs and PtIr (1:3) NPs/CNTs, respectively. For comparison, Pt NPs electrodeposited on the CNTs was prepared by the same procedure as described above, and denoted as Pt NPs/CNTs.

Characterization

The morphology and composition of the PtIr NPs/CNTs nanohybrids were investigated by transmission electron microscopy (JEM-3010) and energy dispersive spectroscopy, respectively. The metal Pt and Ir loading mass for the PtIr NPs/CNTs (or Pt NPs/CNTs) catalyst was determined by inductively coupled plasma-atom emission spectroscopy (Spectro Ciros). The electrochemically active surface area (ESA) of the prepared electrodes was investigated in 0.5 *M* H_2SO_4 solution by cyclic voltammetry. Their electrocatalytic activity toward glucose oxidation was measured in 0.1 *M* KOH+0.05 *M* glucose aqueous solution by CV and CA. All experiments were carried out at room temperature (25 °C). All the potentials reported herein were in respect to SCE.

Results and Discussion

TEM and elemental analysis of PtIr NPs/CNTs nanohybrids

The morphology of PtIr (3:1) NPs/CNTs, PtIr (1:1) NPs/CNTs and PtIr (1:3) NPs/CNTs and Pt NPs/CNTs nanohybrids was characterized by TEM images (Fig. 1). The micrographs in Fig. 1 show that the PtIr and Pt NPs have similar mean particles size with homogeneous dispersion. There is no significant change in the particle size with varying Ir content in the PtIr catalysts. The average particle size of PtIr and Pt NPs and their size distribution were evaluated statistically by measuring the diameter of 100 PtIr or Pt NPs in the selected TEM images. As shown in Fig. 1, the particle size of PtIr and Pt NPs is mainly from 3.0 - 7.0 nm (with an average diameter of ca. 4.0±0.5 nm). In comparison with the results reported previously[35], the addition of glycerol during the electrodeposition process had a distinctly positive effect on dispersion of the Pt or PtIr NPs and reduction of their particle sizes. These results indicate that adding glycerol increased the viscosity of the electrolyte solution and caused decrease in the size of Pt or PtIr clusters by a severe diffusion restriction. The three-dimensional structure of CNTs electrode, small particles size and high dispersion of catalysts NPs may result in large catalyst surface area and good electrocatalytic performance for glucose oxidation.

To confirm the elemental composition of PtIr NPs/CNTs nanohybrids, EDS investigation of PtIr (3:1) NPs/CNTs catalyst was carried out and the corresponding result is shown in Fig. S1 (Supplementary Data). It can be seen that Pt, Ir, O and C are the major elements in the PtIr (3:1) NPs/CNTs catalyst. The carbon peak is located at about 0.3 keV, due to the K electron shell. Oxygen peak at 0.55 keV is probably produced by oxygen containing groups on CNTs. Cu peak is from the testing substrate (Cu foil). The energy peaks of Pt and Ir, located at 2.1 keV (M electron shells), are very close to each other and could not be distinguished, the Pt L signal (L electron shells) is different from that of Ir. The Pt L signal, appears at 9.5 keV for Pt La and at 11.1 keV for Pt Lb. The Ir L signal occurs at 9.1 keV for Ir La and 10.6 keV for Ir Lb. The atomic ratio of Pt/Ir is 2.8, which is close to the theoretical value of 3. The EDS results confirm that PtIr NPs have been successfully deposited on the CNTs surface. Moreover, the total loading mass of Pt or PtIr on glassy carbon electrode measured by the ICP-AES is consistent with those of EDS (Supplementary Data, Table S1).

Electrochemical oxidation of glucose

The electrochemical behavior of PtIr NPs/CNTs and Pt NPs/CNTs nanohybrids was studied by CV. Figure 2 shows the CVs of the electrodes modified with PtIr (3:1) NPs/CNTs, PtIr (1:1) NPs/CNTs, PtIr (1:3) NPs/CNTs and Pt NPs/CNTs nanohybrids in N_2-saturated 0.5 *M* H_2SO_4 aqueous solution. From Fig. 2, it can be observed that the prepared catalysts show similar voltammetric behavior. The PtIr and Pt NPs show signatures of polycrystalline Pt in the potential interval between -0.25 and 0.05 V, which was divided into the reductive absorption region of protons in the reverse cathodic scan and the oxidative desorption region of hydrogen atom in the forward anodic scan[36]. This potential region defined as hydrogen area, i.e., the area of H desorption after the deduction of the double layer region on the CV curves, represents the charge passed for the H desorption, Q_H, and is proportional to the electrochemical active surface area (ESA) of Pt based electrocatalysts. The ESA of PtIr NPs/CNTs and Pt NPs/CNTs nanohybrids can be calculated by the following equation[36]:

$$ESA=Q_H/(0.21\times[Pt])$$

where Q_H (mC cm^{-2}) represents the mean value between the amounts of charge exchanged during the electro-adsorption and desorption of H_2 on Pt sites, [Pt] is the Pt loading (mg cm^{-2}) on the electrode (Supplementary Data, Table S1) and 0.21 (mC cm^{-2}) represents the charge required to oxidize a monolayer of H_2 on bright Pt. The ESA of PtIr or Pt NPs among the

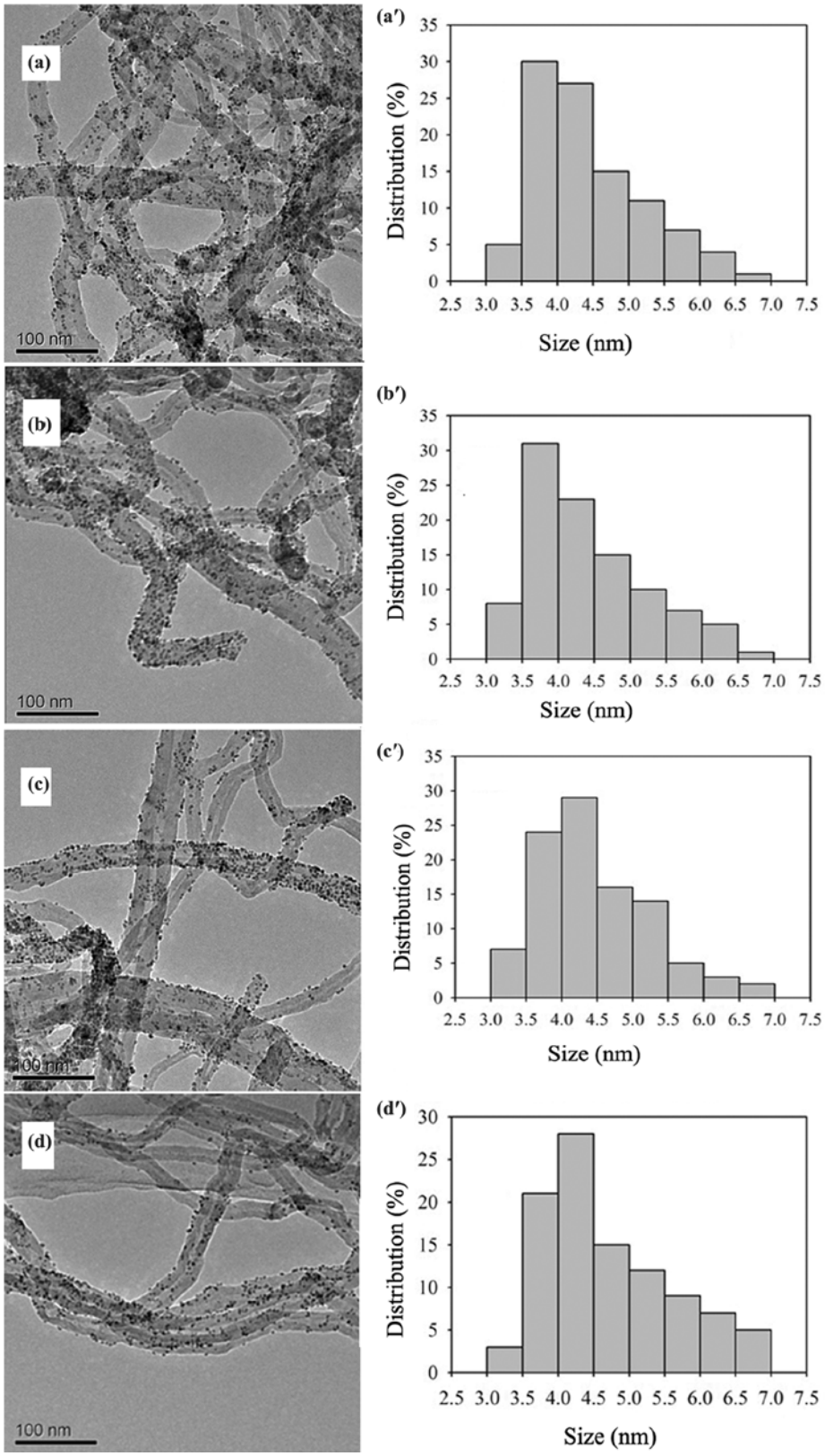

Fig. 1 — TEM images and size distribution of PtIr (Pt) nanoparticles of PtIr (3:1) NPs/CNTs (a, a'), PtIr (1:1) NPs/CNTs (b, b'), PtIr (1:3) NPs/CNTs (c, c') and Pt NPs/CNTs (d, d').

prepared catalysts follows the order of decrease: Pt NPs/CNTs (67.63 m^2 g^{-1}), PtIr (3:1) NPs/CNTs (58.34 m^2 g^{-1}), PtIr (1:1) NPs/CNTs (52.06 m^2 g^{-1}), and PtIr (1:3) NPs/CNTs (43.78 m^2 g^{-1}). It is clear that the ESA of PtIr NPs/CNTs nanohybrids is mostly dependent on the composition of PtIr NPs supported on CNTs; higher the Pt content in PtIr (Pt) NPs, larger is their ESA.

The electrocatalytic activity of as-prepared nanohybrids for glucose oxidation was evaluated in nitrogen-saturated 0.1 *M* KOH+0.05 *M* glucose aqueous solution by cyclic voltammetry, and the cycling was repeated until a reproducible CV curve was obtained. Figure 3 shows the CVs of the electrode modified with PtIr (3:1) NPs/CNTs catalyst in 0.1 *M* KOH aqueous solution in the presence (curve 1) and absence (curve 2) of 0.05 *M* glucose. It can be seen that the current on PtIr (3:1) NPs/CNTs/GC electrode in 0.1 *M* KOH aqueous solution is the representative hydrogen adsorption-desorption and double-layer capacitance on the surface of Pt catalyst. The PtIr (3:1) NPs/CNTs/GC electrode in 0.1 *M* KOH+0.05 *M* glucose aqueous solution exhibit good catalytic activity as evident by multiple polarization peaks attributed to adsorption and redox of glucose and its intermediates. These peaks (Fig. 3, A, B, and C) occur during the positive potential sweep and can be explained by the well-established mechanism of direct electro-oxidation of glucose on Pt electrodes in alkaline media. For convenience, only the anodic oxidation peaks are discussed below. Peak A is ascribed to the chemisorption and dehydrogenation of glucose, and takes place at the hydrogen region (below -0.5 V). With the potential scanning to a more positive value, the adsorbed glucose intermediates are oxidized on the electrode surface, resulting in the small current peak (peak B at *ca.* -0.25 V). When the potential is increased further, the accumulated intermediates block the surface active sites of the PtIr (3:1) NPs/CNTs/GC electrode, which inhibits the electroadsorption of glucose and leads to the sudden drop of current[2, 29]. At potentials beyond -0.05V, the adsorbed intermediates are oxidized, forming products such as gluconolactone or gluconic acid (peak C at *ca.* 0.1 V)[2]. At even higher potential, the formation of metal oxide occurs, and the surface becomes less active, causing the current response to decrease again. For comparison, the CVs of the GC electrode modified with PtIr (3:1) NPs/CNTs, PtIr (1:1) NPs/CNTs, PtIr (1:3) NPs/CNTs and Pt NPs/CNTs in nitrogen-saturated 0.1 *M* KOH+0.05 *M* glucose aqueous solution at a potential scan rate of 50 mV s^{-1} were recorded (Fig. 4). Figure 4 shows that

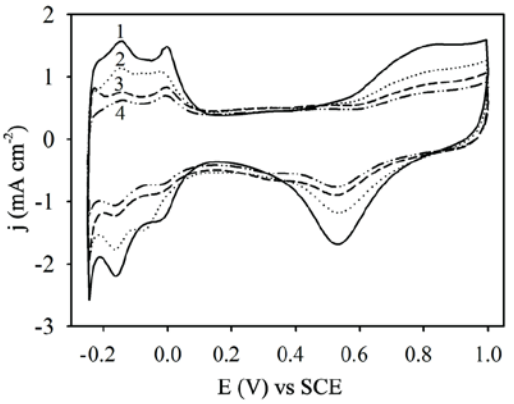

Fig. 2 — Cyclic voltammograms of Pt NPs/CNTs (1), PtIr (3:1) NPs/CNTs (2), PtIr (1:1) NPs/CNTs (3) and PtIr (1:3) NPs/CNTs nanohybrids (4) in nitrogen-saturated 0.5 *M* H_2SO_4 at a scan rate of 50 mV s^{-1}.

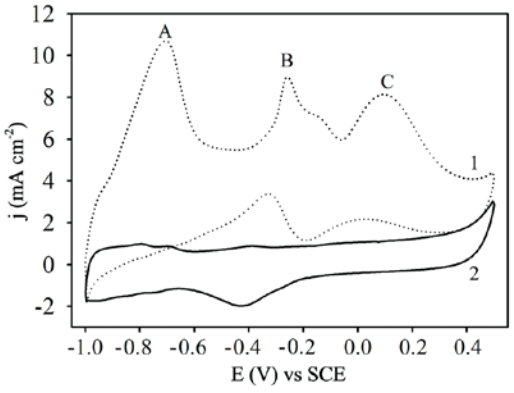

Fig. 3 — Cyclic voltammograms of PtIr (3:1) NPs/CNTs nanohybrids in nitrogen-saturated 0.1 *M* KOH+0.05 *M* glucose aqueous solution (1) and 0.1 *M* KOH solution (2) at a scan rate of 50 mV s^{-1}.

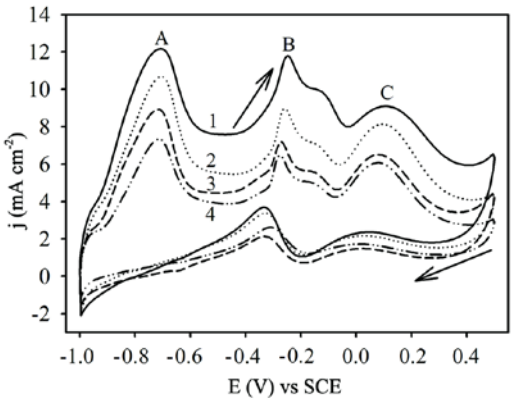

Fig. 4 — Cyclic voltammograms of PtIr (1:1) NPs/CNTs (1), PtIr (3:1) NPs/CNTs (2), PtIr (1:3) NPs/CNTs (3), and Pt NPs/CNTs (4) nanohybrids in nitrogen-saturated 0.1 *M* KOH+0.05 *M* glucose aqueous solution at a scan rate of 50 mV s^{-1}.

all of the electrodes exhibit a current response to glucose oxidation. Since all the tests were performed under the same condition, the current densities of peak B can represent the catalytic activity of the PtIr catalyst for glucose oxidation. PtIr (1:1) NPs/CNTs catalyst has a peak current density of 11.56 mA cm^{-2}, whereas it is only 6.23 mA cm^{-2} for Pt NPs/CNTs catalyst, suggesting that the catalytic activity of PtIr (1:1) NPs/CNTs is 1.86 times higher than that of Pt NPs/CNTs catalyst. The peak current density of PtIr (3:1) NPs/CNTs and PtIr (1:3) NPs/CNTs catalysts are 8.78 mA cm^{-2} and 7.03 mA cm^{-2}, respectively. The electrocatalytic activity for glucose oxidation of PtIr or Pt NPs among the prepared catalysts follows the order of decrease: PtIr (1:1) NPs/CNTs < PtIr (3:1) NPs/CNTs < PtIr (1:3) NPs/CNTs < Pt NPs/CNTs. Clearly, the current densities of glucose oxidation on PtIr NPs/CNTs catalysts are dependent of the Ir content in PtIr catalysts. The best electrocatalytic activity for the electrooxidation of glucose was obtained on the PtIr NPs/CNTs catalysts with Pt/Ir atomic ratio of 1:1. The enhanced catalytic activity can be explained, in part, by the relatively fast oxidation of absorbed CO intermediates by the adjacent Ir. At Pt/Ir atomic ratio of 1:3, the ESA dropped dramatically leading to the reduction in the catalytic activity.

Stability of PtIr NPs/CNTs nanohybrids

The stability of the as-obtained nanohybrids towards glucose oxidation was investigated by chronoamperometric *i-t* test at a fixed potential of -0.1 V for 1200 s in nitrogen-saturated 0.1 *M* KOH+0.05 *M* glucose aqueous solution (Fig. 5). The oxidative current of glucose decreases for all catalysts initially, results from the deactivation of the Pt sites by adsorbed CO species generated from glucose oxidation process. When the processes of accumulation and removal of CO species at Pt sites reach a balance, the current of glucose oxidation at all catalysts stabilizes. Initially faster current decay is seen on the chronoamperometric curve of Pt NPs/CNTs catalysts in contrast with other three catalysts. These results suggest that Pt NPs/CNTs catalysts are more susceptible to the deactivation of Pt sites by adsorbed CO in the absence of Ir. On the other hands, Ir atoms in PtIr alloy can promote oxidation of the surface-absorbed CO to CO_2, leading to activity recovery of the Pt catalysts. The PtIr (1:1) NPs/CNTs catalysts retain a current density of 1.70 mA cm^{-2} at 1200 s, which is much higher than that of PtIr (3:1) NPs/CNTs (1.11 mA cm^{-2}), PtIr (1:3) NPs/CNTs (0.58 mA cm^{-2}) and Pt NPs/CNTs (0.23 mA cm^{-2}), indicating that PtIr (1:1) NPs/CNTs catalyst is more suitable for long-term operations. Five repetitive measurements on PtIr (1:1) NPs/CNTs catalyst gave a standard deviation of 8.2%, showing good reproducibility of the catalyst.

For practical applications, the long-term cycle stability of the catalysts is important. In this work, the long-term cycle stabilities of PtIr (1:1) NPs/CNTs and Pt NPs/CNTs catalysts have also been investigated in 0.1 *M* KOH+0.05 *M* glucose aqueous solution by cyclic voltammetry and the corresponding results are shown in Fig. 6. It can be observed that the value of

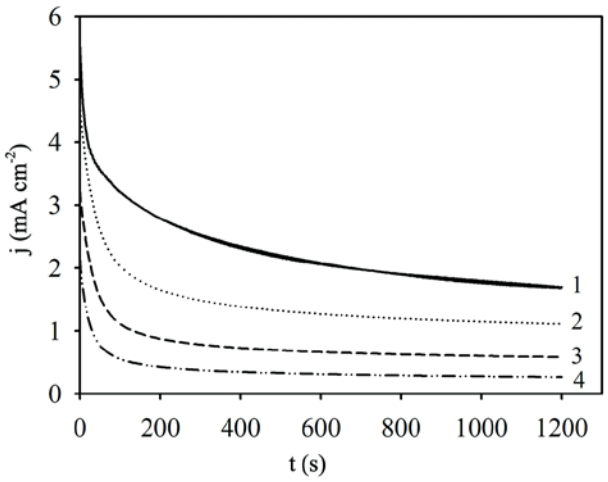

Fig. 5 — Chronoamperometric *i-t* plots of PtIr (1:1) NPs/CNTs (1), PtIr (3:1) NPs/CNTs (2), PtIr (1:3) NPs/CNTs (3), and Pt NPs/CNTs (4) nanohybrids in nitrogen-saturated 0.1 *M* KOH+0.05 *M* glucose aqueous solution.

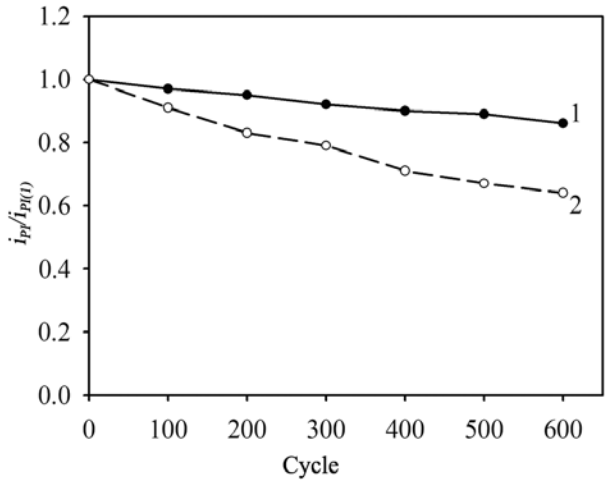

Fig. 6 — Long-term cycle stabilities of PtIr (1:1) NPs/CNTs (1) and Pt NPs/CNTs (2) catalysts in nitrogen-saturated 0.1 *M* KOH+0.05 *M* glucose aqueous solution. [i_{PI}: forward peak current density of peak B; $i_{PI(1)}$: forward peak current density of peak B of the first cycle].

$i_{PI}/i_{PI(1)}$ decreases gradually with the successive scans. In the case of PtIr (1:1) NPs/CNTs nanohybrids, the peak current at 600th cycle is about 86% of that measured at the first cycle. The decrease of $i_{PI}/i_{PI(1)}$ on PtIr (1:1) NPs/CNTs is only 14% for 600 cycles. However, for the Pt NPs/CNTs catalyst, a large decrease (36%) is found. This implies that the long-term stability of PtIr (1:1) NPs/CNTs catalyst is higher than that of the Pt NPs/CNTs catalyst, which agrees with the results of amperometric *i-t* test.

Conclusions

Highly dispersed PtIr NPs were electrodeposited on CNTs by potentiostatic method using 0.5 *M* H_2SO_4+0.5 *M* glycerol aqueous solution with H_2PtCl_6 and H_2IrCl_6 at -0.25 V. The particle size of PtIr NPs catalyst is about 3.0-7.0 nm. The electrocatalytic properties of PtIr NPs/CNTs catalysts with different ratios of Pt:Ir ($R_{Pt/Ir}$), have been investigated by cyclic voltammetry in 0.1 *M* KOH+0.05 *M* glucose aqueous solution. A higher peak current was observed at PtIr NPs/CNTs/GC electrodes than at Pt NPs/CNTs/GC electrodes. The results of CVs show that the PtIr (1:1) NPs/CNTs/GC electrode exhibits better electrocatalytic activity than PtIr (3:1) NPs/CNTs/GC, PtIr (1:3) NPs/CNTs/GC and Pt NPs/CNTs/GC electrodes. Additionally, the PtIr catalysts prepared herein also show a better long-term cycling stability towards glucose oxidation than pure Pt NPs on CNTs surface. The developed PtIr NPs/CNTs nanohybrids are promising catalysts for direct glucose fuel cells.

Supplementary Data

Supplementary Data associated with this article are available in the electronic form at http://www.niscair.res.in/jinfo/ijca/IJCA_56A(10)1007-1013_SupplData.pdf.

Acknowledgment

This work was financially supported by the National Natural Science Foundation of China (21303134) and Natural Science Foundation of Shaanxi Province, China (2014JQ2046).

References

1 Elouarzaki K, Le Goff A, Holzinger M, Thery J & Cosnier S, *J Am Chem Soc*, 134 (2012) 14078.
2 Habrioux A, Sibert E, Servat K, Vogel W, Kokoh K B & Alonso-Vante N, *J Phys Chem B*, 111 (2007) 10329.
3 Yan X, Ge X & Cui S, *Nanoscale Res Lett*, 6 (2011) 1.
4 Park S, Song Y J, Han J-H, Boo H & Chung T D, *Electrochim Acta*, 55 (2010) 2029.
5 Pasta M, La Mantia F & Cui Y, *Electrochim Acta*, 55 (2010) 5561.
6 Quan H, Park S-U & Park J, *Electrochim Acta*, 55 (2010) 2232.
7 Yang Y J & Hu S, *Electrochim Acta*, 55 (2010) 3471.
8 Calabrese B S, Gallaway J & Atanassov P, *Chem Rev*, 104 (2004) 4867.
9 Cracknell J A, Vincent K A & Armstrong F A, *Chem Rev*, 108 (2008) 2439.
10 Kavanagh P, Boland S, Jenkins P & Leech D, *Fuel Cells*, 9 (2009) 79.
11 Raitman OA, Katz E, Bückmann AF & Willner I, *J Am Chem Soc*, 124 (2002) 6487.
12 Willner I, Yan Y M, Willner B & Tel-Vered R, *Fuel Cells*, 9 (2009), 7.
13 Meng L, Jin J, Yang G, Lu T, Zhang H & Cai C, *Anal Chem*, 81 (2009) 7271.
14 Wu B H, Hu D, Kuang Y Y, Liu B, Zhang X H & Chen J H, *Angew Chem Int Ed*, 48 (2009) 4751.
15 Rao M L B & Drake R F, *J Electrochem Soc*, 116 (1969) 334.
16 Delidovich I, Taran O P & Matvienko L G, *Catal Lett*, 140 (2010) 14.
17 Chen C C, Lin C L & Chen L C, *Electrochim Acta*, 152 (2010) 408.
18 Liu S M, Zheng Y D & Cui L Y, *Adv Mat Res*, 1095 (2015) 299.
19 Cai Z X, Liu C C, Wu G H, Chen X M & Chen X, *Electrochim Acta*, 112 (2013) 756.
20 Beden B, Largeaud F, Kokoh K B & Lamy C, *Electrochim Acta*, 41 (1996) 701.
21 Balcazar M G, Acosta D M, Castaneda F, Garcia J L & Arriaga L G, *Electrochim Commun*, 12 (2010) 864.
22 Liang W & Zhuobin Y, *Sensors*, 3 (2003) 544.
23 Liu Z, Huang L & Zhang L, *Electrochim Acta*, 54 (2009) 7286.
24 Wang J, Thomas D F & Chen A, *Anal Chem*, 80 (2008) 997.
25 Li L H, Zhang W D & Ye J S, *Electroanal*, 20 (2008) 2212.
26 Xiao F, Zhao F, Mei D, Mo Z & Zeng B, *Biosens Bioelectron*, 24 (2009) 3481.
27 Mahshid S S, Mahshid S, Dolati A, Ghorbani M, Yang L & Luo S, *J Alloy Compd*, 554 (2013) 169.
28 He B, Hong L, Lu J, Hu J, Yang Y & Yuan J, *Electrochim Acta*, 91 (2013) 353.
29 Holt-Hindle P, Nigro S, Asmussen M & Chen A, *Electrochem Commun*, 10 (2008) 1438.
30 Wu B, Kuang Y, Zhang X & Chen J, *Nano Today*, 6 (2011) 75.
31 Chu Y Y, Wang Z B, Gu D M & Yin G P, *J Power Sources*, 195 (2010) 1799.
32 Jiang F, Yao Z, Yue R, Du Y, Xu J & Yang P, *Int J Hydrogen Energy*, 37 (2012) 14085.
33 Maiyalagan T, *Int J Hydrogen Energy*, 34 (2009) 2874.
34 Quinn B M, Dekker C & Lemay S G, *J Am Chem Soc*, 127 (2005) 6146.
35 He Z B, Chen J H, Liu D Y, Tan H, Deng W & Kuang Y F, *Mater Chem Phys*, 85 (2004) 396.
36 Pozio A, De Francesco M, Cemmi A, Cardellini F & Giorgi L, *J Power Sources*, 105 (2002) 13.